

Controlling Nanoparticle Aggregation in Colloidal Microwave Absorbers via Interface Chemistry

Brian A. Larsen^a, Michael A. Haag^a, Michael H. B. Stowell^b, David C. Walther^c, Albert P. Pisano^c,
Conrad R. Stoldt*^a

^aDept. of Mechanical Engineering, University of Colorado, Boulder, CO, USA 80309-0427;

^bDept. of Molecular, Cellular, and Developmental Biology, University of Colorado, Boulder, CO,
USA 80309;

^cDept. of Mechanical Engineering, University of California at Berkeley, Berkeley, CA, USA 94720

ABSTRACT

Interface chemistry can be implemented to modulate the aggregation and dispersion of nanoparticles in a colloidal solution. In this experimental study, we demonstrate the controlled aggregation of superparamagnetic magnetite nanoparticles in organic and aqueous solutions. With decrease in solution pH, individual nanoparticles (12-14 nm) reproducibly cluster to form ~52 nm monodisperse aggregates in toluene. Spin-spin (T₂) proton relaxation measurements of the micellated clusters before and after aggregation show a change in the molar relaxation rate from 303 sec⁻¹mol⁻¹ to 368 sec⁻¹mol⁻¹ for individual and clustered nanoparticles, respectively. DNA-mediated aggregation of micellated nanoparticles in the colloidal solution is also demonstrated where the number of single-stranded DNA per particle determines the ultimate size of the nanoparticle aggregate.

Keywords: Nanoparticle, magnetite, colloid, DNA, microwave, relaxation

1. INTRODUCTION

Microwave absorbing materials for military applications have been investigated since the advent of radar systems. The majority of these systems, including Salisbury screens, Jaumann absorbers, radar absorbing paints, and particle laden polymeric layers, are passive in nature. There is some work with active surfaces such as variable impedance surfaces or other tunable microwave absorbers [1] and can be thought of as switched Jaumann absorbers. Furthermore, there is at least one system described in the literature [2] that modifies the change of the permittivity of an absorbing layer by introduction of a high permittivity liquid into a porous matrix of lower permittivity. The electrostatic actuation of conducting polymers can also be utilized to actively modify the absorption characteristics via application of a low strength DC bias field. The work of Wright and coworkers [3] has examined the absorptivity of polyethylene oxide polymer absorber that contains both polyaniline tetrafluoroborate and silver. More recent work with poly(3,4-ethylenedioxythiophene) and copper metal in a polyethylene LiBF₄ polymer electrolyte matrix show that an electrical DC bias across the absorbing layer is an effective tuning mechanism for modulation of the reflected microwave signal [4]. Additional passive methods which utilize intricate miniature inductive and capacitive circuits have been demonstrated [5], however these designs have a large cost associated with their fabrication processes and limited design geometries.

Recently, the feasibility of ferromagnetic nanoparticle composites for microwave absorption has been theoretically described [6, 7] and demonstrated experimentally [8, 9]. Highly efficient absorption is predicted because the composite combines the advantages of two absorbers, namely, ferromagnetic particles and a dielectric matrix. When surface area is limited (e.g., the wing of a small aircraft), the design of a good absorber becomes very difficult since precise control over some magnetic and dielectric properties is often necessitated, and conventional materials become challenging if not impossible to integrate into the design (especially at reduced scales). A composite absorber that utilizes ferromagnetic particles in combination with a dielectric matrix material offers the most flexibility for design and properties control, as the composite can be tuned and optimized via changes in both the ferromagnetic inclusions and the surrounding matrix. Ultra-small superparamagnetic (SPM) particles possess the most effective microwave absorption cross-sections [6], and through small changes in size or composition, the absorption frequency can be shifted. Similarly, the dielectric matrix can be tuned synthetically to enhance absorption. Finally, the composite as a whole can be tuned through changes in the

particle volume fraction, which is demonstrated to modulate the reflected intensity of the microwave. This increase in absorption can be manifested in layers with thickness less than $\lambda/4$.

Bregar's theoretical efforts [6] indicate that the microwave reflectivity of such a nanoparticle composite can be tuned through changes in particulate volume fraction, composition, and size, or through changes in the dielectric constant of the matrix material. Experimental validation of this approach is shown by Pinho and coworkers [9], where reflection loss from a composite composed of a ~500 nm sized Co-TiBa hexaferrite filler in a polychloroprene elastomeric matrix is experimentally demonstrated in the 8-16 GHz bandwidth. Other recent work has determined the amount of RF shielding of various SPM particles (Fe_3O_4 , $\text{MnZnFe}_2\text{O}_4$, and CoFe_2O_4) in polymer matrices at similar frequencies [8].

While the current experimental approaches to fixed nanoparticle composite absorbers show promise, there are several potential limitations that can be improved upon. First, the typical nanoparticle size distribution is broad and the average particle size is large. The combination of these properties yields broad and poorly defined absorption bands with a small absorption cross-section. The dielectric characteristics of solid-state thin film matrices such as polymers can be tuned via material selection, but their relatively rigid nature, larger overall mass, and the difficulties associated with generating disperse nanoparticle composites create some fabrication and deployment problems. To achieve truly narrowband absorber performance, the particles should be well distributed within the matrix and this is not easily achieved in current studies [9]. Furthermore, real-time tuning of the composite's absorption becomes difficult or impossible when the solid matrix and particle inclusions are fixed. A thin film composite can be actuated mechanically, electrostatically, etc. to achieve modulation of film properties and consequently the absorption cross-section, but this approach could entail the integration of additional sophisticated actuators that require additional metallization, power, volume and mass on the absorbing structure.

This work describes experimental efforts toward the development of microwave absorbers composed of nanoparticulate inclusions in a liquid matrix. In a colloidal RF absorber, the absorbance cross-section can be tailored through changes in size, composition, morphology and density of the nanoparticle inclusions [6]. These material properties can be accurately controlled through the particle synthesis process. Furthermore, the absorbance characteristics of the colloid can be tailored via choice of an appropriate liquid matrix in which the inclusions are suspended. With the choice of a liquid matrix containing unbound inclusions, the feasibility of modulation of RF absorption becomes possible without the use of mechanical or electrostatic actuation. Instead, absorption changes can be realized through application of chemically selective surface ligands such as biomolecules to the nanoparticle surfaces. These site-specific ligands can dictate particle aggregation and dissolution in the colloid, thus modulating the local absorption characteristics through changes in the particle volume fraction and the magnetic properties of the colloid. In this paper, progress toward colloidal systems of this nature with an emphasis on the synthesis of magnetite (Fe_3O_4) nanoparticle absorbers and the implementation of particle surface chemistries that promote controlled aggregation of the colloid inclusions is noted. Specifically, details are provided regarding efforts to control particle aggregation and dissolution via changes in solution pH and through the use of selective DNA interactions between particles. These approaches are a first step toward the development of 'smart' absorbers engineered to operate reversibly and autonomously without external mechanical or electrostatic actuation.

2. MATERIALS AND METHODS

2.1 Synthesis and characterization of Fe_3O_4 nanoparticles

Triethylamine (98%), Fe(III)-acetylacetonate (further referred to as $\text{Fe}(\text{Acac})_3$, 97%), heptanoic acid (99%), anhydrous toluene (99.8%), and ethanol were purchased from Sigma-Aldrich. All chemicals were used as purchased from the manufacturer and no further purification steps were taken. Fe_3O_4 nanoparticles were synthesized by heating 18.6 mL triethylamine and 1.4 mL heptanoic acid (20% molar concentration) to reflux (260°C) under nitrogen gas in a three necked round bottom flask. The solution was mixed using a magnetic stir bar. Upon reaching temperature, 0.045 M $\text{Fe}(\text{Acac})_3$ was carefully added to the solvent. To initiate particle nucleation, 14 psi oxygen gas was introduced into the reaction vessel for 5 sec. Subsequently, the solution turns a dark brown/black color, indicative of the formation of Fe_3O_4 nuclei. The experiment was halted after one hour and the resulting product was a black precipitate with a clear supernatant. The product was centrifuged at 4000 RPM for 15 minutes and washed three times in toluene to remove the excess organic material (Allegra X-22, SX4250 Rotor, Beckman Coulter). The final product was Fe_3O_4 nanoparticles suspended in toluene with a heptanoic acid (stabilizing agent) surface termination.

Powder X-ray diffraction (XRD), transmission electron microscopy (TEM), and high-resolution TEM (HRTEM) are performed on the Fe₃O₄ product to determine product size, the particle size distribution (PSD), and crystal structure. Powder XRD measurements were obtained using a Scintag Pad V diffractometer equipped with a Cu K radiation source. TEM micrographs were obtained on a Philips CM10 operating at 80 kV. Further details on the material synthesis, characterization, and magnetic properties of the resulting Fe₃O₄ product are described elsewhere [10].

2.2 Carboxylated micellation of Fe₃O₄ nanoparticles

Heptanoic acid capped Fe₃O₄ nanoparticles in toluene were added to 1,2-Distearoyl-sn-Glycero-3-Phosphoethanolamine-N-[Carboxy(Polyethylene Glycol)2000] in chloroform at a 1:1.8 ratio of nanoparticles to phospholipids (w/w). The nanoparticle/phospholipid solution was dried under nitrogen gas and subjected to vacuum for 2 hours to remove organic solvents, yielding a film of nanoparticles and solid phospholipids. Deionized water was added to the nanoparticle/phospholipid film at a magnetite/water concentration of 1 mg/ml and the solution was bath sonicated. The resulting colloid of micellar magnetite nanoparticles was filtered using 0.1 μm Whatman inorganic syringe filters to remove particulates. This procedure was adapted from previously published methods [11].

2.3 Fe₃O₄ micelle size and aggregation measurements

Fe₃O₄ nanoparticle micelle encapsulation was studied using TEM and negative phospholipid staining. Approximately 10 μl of magnetite micelle solution was deposited on a carbon TEM grid, and approximately 10 μl of 5% (w/v) phosphotungstic acid solution was added. The sample was allowed to dry and was imaged using a Philips CM10 TEM operating at 80 kV. This procedure was adapted from previously published methods for quantum dots and magnetite nanoparticles [11, 12]. Extent of aggregation and additional size measurement of the Fe₃O₄ micelles and Fe₃O₄ nanoparticles was performed using a Brookhaven dynamic light scattering (DLS) system. Cuvettes were rinsed for dust using DI water or toluene, depending on the sample solvent, filtered through 0.02 μm Whatman syringe filters and Fe₃O₄ micelles were filtered through 0.1 μm Whatman inorganic syringe filters. Fe₃O₄ micelles were studied in DI water, and pre-micellation nanoparticles were studied in toluene. All samples were measured at room temperature.

2.4 Carboxylated micelle crosslinking to DNA

Amine/Biotin functionalized DNA oligonucleotides (oligos) were crosslinked to the carboxylated micelles using 1-Ethyl-3-[3-dimethylaminopropyl]carbodiimide hydrochloride (EDC), an amine-carboxyl crosslinker. The following DNA oligos were obtained from Invitrogen; 5' Amino-TGGGTGTTGAGAGGCTGGC-Biotin 3', 5' Amino-GCCAGCCTCTCAACACCCA-Biotin 3'. Oligos were dissolved in 10 mM Phosphate Buffer pH 7.4 at 100 μM concentration. Samples were stored at -20°C. Carboxyl terminated micelle incorporated nanoparticles were dissolved in 10 mM Phosphate buffer, 1 mM EDTA, pH 7.4 at a concentration of 6 nM. Oligos and nanoparticles were mixed at vary ratios from 1(DNA) to 1(NP) to 100(DNA) to 1(NP) in 500 uL of phosphate buffer and EDC was added to a concentration of 1 mg/mL. The reaction was allowed to proceed at room temperature for 2 hours at which point the particles were pelleted and washed using centrifugation.

Samples for electron microscopy were applied to a freshly carbon coated, glow-discharged EM grid and washed with distilled water twice. Images were recorded at a magnification of 5800 and at a defocus of 5m using a Phillips CM10 microscope, equipped with a LaB6 gun and operating at 100 keV. Images were recorded with a Gatan 1K X 1K CCD camera. Average particle cluster numbers were determined from 5 randomly chosen images.

2.5 Spin-spin proton relaxation measurement

Spin-spin (T₂) proton relaxation measurements were obtained on a Varian 300 MHz nuclear magnetic resonance (NMR) spectrometer. Carboxylated micelles were divided in three dilutions and 10 μl samples were prepared in sealed microcapillary tubes. Each sample was analyzed using a Carr-Purcell-Meiboom-Gill pulse sequence to determine the T₂ relaxation time. Molar relaxation rates were determined by a determining the linear slope of the inverse T₂ relaxation times and Fe₃O₄ molarity (1/T₂ vs. molarity). Fe₃O₄ molarity for each dilution was determined by inductively coupled plasma optical emission spectrometry.

3. RESULTS AND DISCUSSION

3.1 Multi-particle micelle encapsulation

In this section, we describe the development of a micelle encapsulation procedure that allows control of aggregate size via changes in solution pH during processing. In principle, this procedure is reversible by titration of the colloidal solution with either a weak Lewis acid or base. To characterize the aggregated nanoparticles in the colloid, we perform DLS and spin-spin proton relaxation measurements to link changes in aggregate size with magnetic behavior. As discussed in Section 1, changes in SPM nanoparticle aggregate size within the matrix should modify the measured RF absorption from the composite system. Previous work has demonstrated that the volume fraction of SPM nanoparticles dispersed in a matrix can increase the RF absorption signal due to dipole-dipole interactions between individual particles in an aggregate and spin coupling between particle aggregates [13]. As a consequence, SPM nanoparticles such as Fe_3O_4 in the aggregated state possess higher magnetization that induces a faster dephasing of proton spins (higher R2 relaxation rates, shorter T2 relaxation times) in the vicinity of the agglomerate [14, 15].

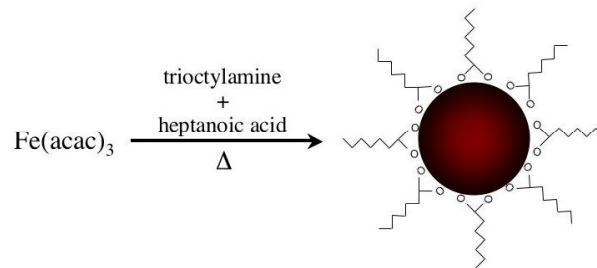


Fig. 1. Schematic showing the synthesis of a Fe_3O_4 particle from $\text{Fe}(\text{Acac})_3$ in trioctylamine and heptanoic acid. Following the synthesis, the particle is capped with the heptanoic acid molecule and suspended in toluene solution.

In Fig. 1, Fe_3O_4 nanoparticles capped with heptanoic acid are schematically shown and a TEM image of the typical Fe_3O_4 final product is shown in Fig. 2a. In the Fe_3O_4 /toluene colloid, particle aggregation is achieved by lowering the pH of the toluene solution. The carboxylic acid capping agent coordinates to the surface of the metal oxide via the deprotonated carboxyl group. The bare metal oxide surface is an electron donor (Lewis base) [16], and consequently coordinates with the de-protonated heptanoic acid molecule in toluene solution. Heptanoic acid is removed from the particle surface by lowering the solution pH with a weak Lewis acid (such as acetic acid), which re-protonates the carboxyl group in toluene. As a consequence, the inherently hydrophilic surfaces of the metal oxide nanoparticles are exposed to the hydrophobic toluene solution and begin to cluster without the capping molecule, thus forming the larger nanoparticle aggregate. Conversely, the nanoparticles can be de-aggregated by titrating the Fe_3O_4 /toluene colloid with a weak Lewis base (such as THF). The pH-mediated aggregation of Fe_3O_4 nanoparticles in organic solution was adapted from previously published studies on iron particle dispersion [17].

The as-synthesized nanoparticles were processed in toluene at neutral and reduced pH followed by phospholipid encapsulation, yielding single and multi-particle micelles, respectively. Phospholipid micellation lends stability and water solubility for evaluation by DLS and NMR, as well as terminal functional groups for subsequent bioconjugation (further described in Section 3.2). In Fig. 2b, single particles processed at neutral pH are shown following micelle encapsulation. The DLS size distribution results shown in Fig. 3 demonstrate pH dependent aggregation of Fe_3O_4 nanoparticles encapsulated in phospholipid micelles. The ~ 16 nm mean sample diameter is consistent with monodisperse single particle micelles with a magnetite core of approximately 12-14 nm (Fig. 2b). The ~ 52 nm mean sample diameter is consistent with nanoparticle aggregates containing approximately 48 nanoparticles each, assuming a packing fraction of 0.74 (close-packed) and individual particle diameters between 12-14 nm. Both size distributions demonstrate negligible skew and were reproducible during multiple DLS acquisitions.

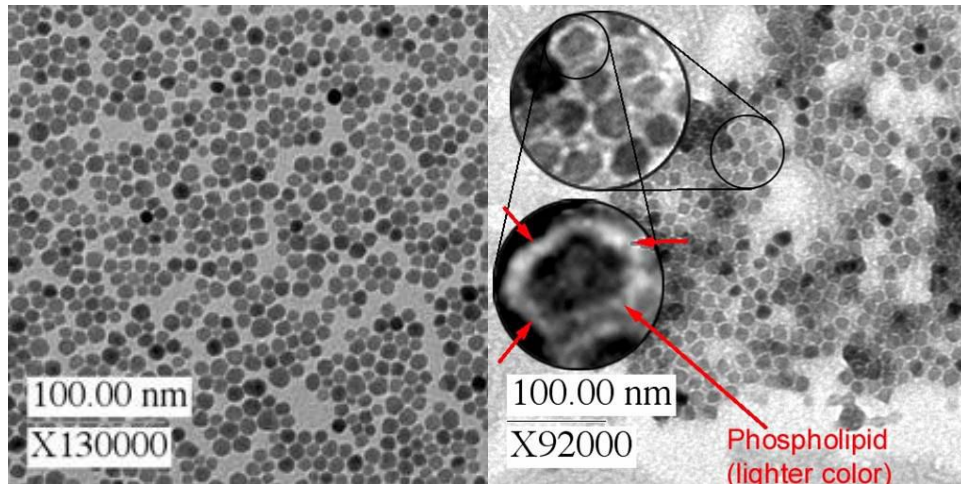


Fig. 2. TEM images showing (a, left) as-synthesized 12 nanometer diameter Fe_3O_4 particles and (b, right) Fe_3O_4 nanoparticles following encapsulation in a phospholipid micelle.

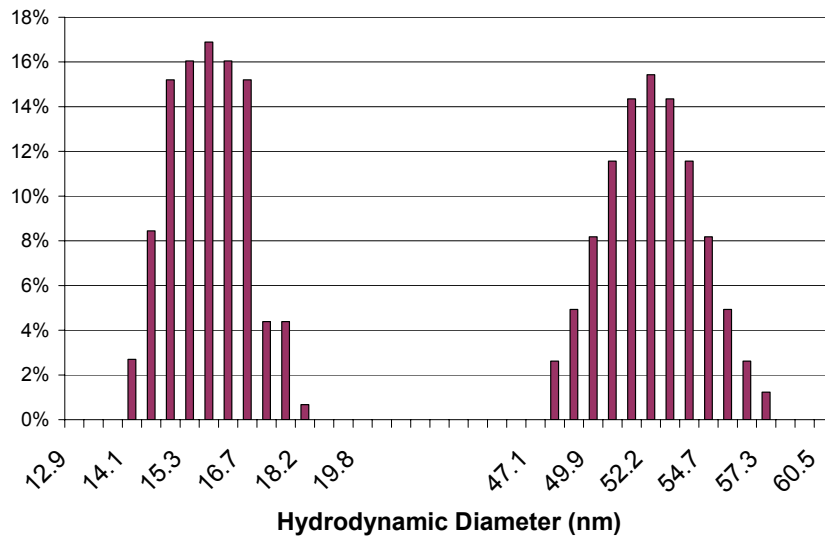


Fig. 3. Distribution for the hydrodynamic diameters of SPM Fe_3O_4 nanoparticles after phospholipid micellation. Left: Single particles processed at neutral pH (~ 16 nm mean diameter). Right: Multi-particle aggregates processed at reduced pH (~ 52 nm mean diameter).

T2 relaxation results for the single and multi-particle micelles shown in Fig. 4 demonstrates the enhanced molar T2 relaxation rate of the multi-particle micelles compared to single particle micelles. The $368 \text{ sec}^{-1} \cdot \text{mol}^{-1}$ T2 relaxation rate of the multi-particle micelle sample shows a 22% increase compared to the $303 \text{ sec}^{-1} \cdot \text{mol}^{-1}$ T2 relaxation rate for the single particle micelle sample. The higher T2 relaxation rate for the multi-particle sample is consistent with Fe_3O_4 multi-particle encapsulation results published by other investigators using a different aggregation route [18]. The molar relaxation rates were obtained from the linear fits of the inverse T2 measurements for three Fe_3O_4 micelle dilutions. Both linear fits demonstrated near ideal correlation ($R^2 > 0.9$). As demonstrated by the plot in Fig. 4, the larger aggregate of magnetic material per micelle in water yields a higher molar relaxation rate than the single nanoparticle per micelle colloidal sample.

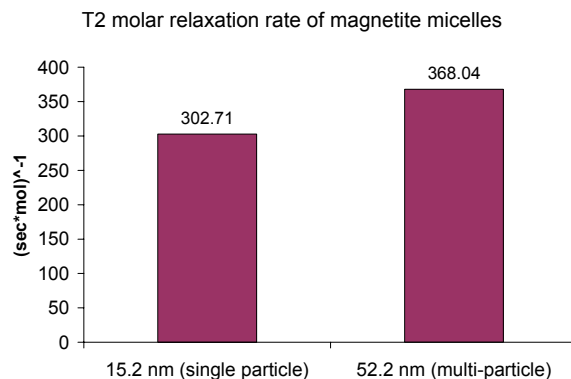


Fig. 4. Hydrodynamic diameter (nm) of the Fe₃O₄ nanoparticle micelles plotted versus T2 molar relaxation rate. The larger nanoparticle aggregate yields a higher molar relaxation rate than individual particles.

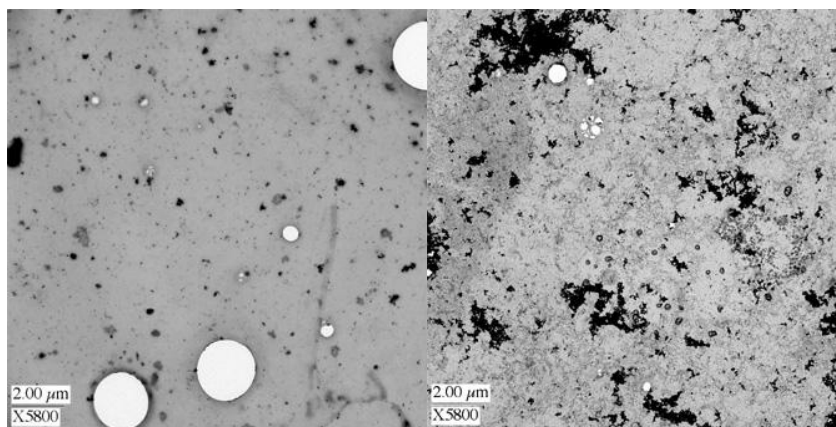


Fig. 5. TEM images showing DNA mediated aggregation of micelle-encapsulated particles (a, left) before hybridization and (b, right) after hybridization. In (b), fractal aggregates larger than 1μm in diameter are observed.

3.2 DNA-mediated nanoparticle aggregation

In this section, we describe a second experimental approach for promoting nanoparticle aggregation in the colloidal solution mediated by DNA. Several studies have investigated the bimolecular driven aggregation of micro and nanoparticles in solution [14, 19]. In our case, particle aggregation is desired to modulate local number concentration and in turn RF absorption in the colloidal solution. Of particular interest is exploring the use of single-stranded DNA (ssDNA) to drive particle aggregation. Because there is a very well defined relationship between DNA sequence and the thermodynamics of double-stranded DNA (dsDNA) formation, it is possible to control the aggregation of particles using sequence specificity [14]. dsDNA melting transitions are well defined and correlate with the DNA nucleotide sequence. Melting temperatures increase with increasing DNA strand length and with increasing GC base content, and are easily calculated from the sequence using pair wise interaction parameters [20]. The melting transitions of these dsDNA are typically broad and occur over a temperature range of ~20°C. Recently it has been observed that dsDNA transitions in micro- or nanoparticle aggregates show sharp thermal transitions of a few degrees or less [21, 22], with time constants in the millisecond range for sufficient temperature jumps [23]. Thus, the DNA driven aggregation, thermal melting, and dissolution of colloidal nanoparticles can be controlled over a very sharp thermal range yielding reversible changes in particle volume fraction.

In the work reported here, we link ssDNA to a population of micelle-encapsulated particles via carboxyl functional groups on the phospholipid molecules. The complimentary ssDNA to the former is bound to a second population of

micelle-encapsulated particles. Upon mixing of the two populations in the colloidal solution at 20°C, the complimentary DNA strands hybridize, thus promoting aggregation below the melting transition of the dsDNA. By varying the ratio of ssDNA per micelle, the ultimate size of the aggregate can be tailored. For example, by maximizing the number of ssDNA attached to each population (saturation of ssDNA per micelle), aggregation is not well-controlled and extremely large aggregate networks form. Fig. 5 shows TEM images before and after DNA hybridization and formation of fractal aggregates with sizes in excess of 1 μm .

In order to demonstrate precise control of the bioconjugation process and aggregate formation, ssDNA was linked to micelle-encapsulated particles as described in Section 3.1 in ratios of one strand per micelle (1:1) and 2.5 strands per micelle (2.5:2.5) on average. Figure 6 shows size data obtained by DLS for samples with no aggregation, and micelle-encapsulated particle populations with 1:1 and 2.5:2.5 DNA additions per micellated particle. For the case of moderate aggregation, a 1:1 DNA to micelle ratio should yield on average only two micelles per aggregate, while a 2.5:2.5 DNA to micelle ratio should yield a larger aggregate. The results shown in Fig. 6 support this conclusion, as the (1:1) sample has a hydrodynamic diameter 50% greater than the unhybridized micelle, indicative of the decreased diffusion coefficient of aggregated particles. Similarly, the (2.5:2.5) sample has a hydrodynamic diameter nearly 150% greater than the unhybridized micelle, demonstrating increased aggregation. These results indicate that DNA can be utilized as a selective surface ligand on nanoparticles to precisely control the degree of aggregation in colloidal systems. Future work will demonstrate reversibility in DNA-mediated aggregate systems by thermally annealing the colloid above the DNA melting transition to disperse the aggregates and correlate these changes to the measured molar T2 relaxation rate.

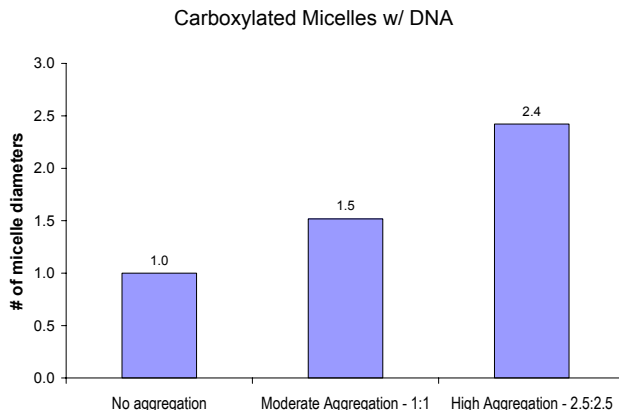


Fig. 6. DLS results for particle micelles conjugated with varying quantities of complimentary DNA. Note that the diameters are normalized to diameter of single micelles.

4. CONCLUSIONS

In this work, two routes to the controlled aggregation of nanoparticulate inclusions in a colloidal solution have been demonstrated. In both scenarios, nanoparticle interface chemistry is used to dictate the degree of aggregation without the application of external mechanical or electrostatic actuation. In the first case, we utilized a pH change in the colloidal solution and acid-base interaction of the molecular capping layer to drive nanoparticle aggregation (and dispersion). T2 relaxation measurements on the resulting aggregates demonstrate magnetic property changes with local nanoparticle concentration. In the second case, we demonstrated aggregation in the colloid via the hybridization of complimentary ssDNA covalently bound to the surfaces of two particle populations. The ultimate aggregate size and shape is controlled by the amount of ssDNA per particle, thus demonstrating that aggregate size can be precisely tailored via the addition of a site-specific biological ligand such as DNA. In principle, both of the interface chemistries demonstrated in this paper are both passive and reversible. The quantification of these effects will be carried out in future research studies.

REFERENCES

- [1] M. D. Bushbeck and C. H. Chan, "A tuneable, switchable dielectric grating," *Microwave and Guided Wave Letters*, IEEE [see also *IEEE Microwave and Wireless Components Letters*], vol. 3, pp. 296-298, 1993.
- [2] M. Bushbeck, "Electromagnetic scattering from a two-state phase switched screen using a control impedance," 2004.
- [3] P. V. Wright, B. Chambers, A. Barnes, K. Lees, and A. Despotakis, "Progress in smart microwave materials and structures," *Smart Materials & Structures*, vol. 9, pp. 273-279, 2000.
- [4] R. Zhang, A. Barnes, K. L. Ford, B. Chambers, and P. V. Wright, "A new microwave 'smart window' based on a poly(3,4-ethylenedioxythiophene) composite," *Journal of Materials Chemistry*, vol. 13, pp. 16-20, 2003.
- [5] M. Wilson, "Designer materials render objects nearly invisible to microwaves," in *Physics Today*, vol. 60, 2007, pp. 19-23.
- [6] V. B. Bregar, "Advantages of ferromagnetic nanoparticle composites in microwave absorbers," *Magnetics*, IEEE Transactions on, vol. 40, pp. 1679-1684, 2004.
- [7] V. B. Bregar, "Effective-medium approach to the magnetic susceptibility of composites with ferromagnetic inclusions," *Physical Review B (Condensed Matter and Materials Physics)*, vol. 71, pp. 174418-8, 2005.
- [8] R. P. Pant, S. K. Halder, S. K. Dhawan, J. Shah, V. Kumar, and N. D. Kataria, "Microwave Absorption Studies on Ferrofluid-Conducting Polymer Composite," presented at XXVIIIth General Assy of Int'l Union of Radio Science, New Dehli, India, 2005.
- [9] M. S. Pinho, M. L. Gregori, R. C. R. Nunes, and B. G. Soares, "Performance of radar absorbing materials by waveguide measurements for X- and Ku-band frequencies," *European Polymer Journal*, vol. 38, pp. 2321-2327, 2002.
- [10] A. J. Barker, B. Cage, S. Russek, and C. R. Stoldt, "Ripening during magnetite nanoparticle synthesis: Resulting interfacial defects and magnetic properties," *Journal of Applied Physics*, vol. 98, 2005.
- [11] N. Nitin, L. E. W. LaConte, O. Zurkiya, X. Hu, and G. Bao, "Functionalization and peptide-based delivery of magnetic nanoparticles as an intracellular MRI contrast agent," *Journal of Biological Inorganic Chemistry*, vol. 9, pp. 706-712, 2004.
- [12] B. Dubertret, P. Skourides, D. J. Norris, V. Noireaux, A. H. Brivanlou, and A. Libchaber, "In vivo imaging of quantum dots encapsulated in phospholipid micelles," *Science*, vol. 298, pp. 1759-1762, 2002.
- [13] N. Guskos, J. Typek, T. Bodziony, Z. Roslaniec, U. Narkiewicz, M. Kwiatkowska, and M. Maryniak, "Temperature dependence of FMR field of magnetic nanoparticles/polymer composite," *Reviews on Advanced Materials Science*, vol. 12, pp. 133-138, 2006.
- [14] J. M. Perez, L. Josephson, T. O'Loughlin, D. Hogemann, and R. Weissleder, "Magnetic relaxation switches capable of sensing molecular interactions," *Nature Biotechnology*, vol. 20, pp. 816-820, 2002.
- [15] A. Roch, R. N. Muller, and P. Gillis, "Theory of proton relaxation induced by superparamagnetic particles," *Journal of Chemical Physics*, vol. 110, pp. 5403-5411, 1999.
- [16] E. Johansson and L. Nyborg, "XPS study of surface-active organic compounds on fine ferrous powder," *Surface and Interface Analysis*, vol. 30, pp. 333-336, 2000.
- [17] W. J. Chen, S. S. Wong, W. G. Peng, and C. D. Wu, "Effect of Acid-Base Interaction on Magnetic Dispersion Containing Alpha-Fe Metal Particles," *Ieee Transactions on Magnetics*, vol. 27, pp. 4648-4650, 1991.
- [18] B. A. Moffat, G. R. Reddy, P. McConville, D. E. Hall, T. L. Chenevert, R. R. Kopelman, M. Philbert, R. Weissleder, A. Rehemtulla, and B. D. Ross, "A novel polyacrylamide magnetic nanoparticle contrast agent for molecular imaging using MRI," *Mol Imaging*, vol. 2, pp. 324-32, 2003.
- [19] T. A. Taton, C. A. Mirkin, and R. L. Letsinger, "Scanometric DNA array detection with nanoparticle probes," *Science*, vol. 289, pp. 1757-1760, 2000.
- [20] H. T. Allawi and J. SantaLucia, "Thermodynamics and NMR of internal GT mismatches in DNA," *Biochemistry*, vol. 36, pp. 10581-10594, 1997.
- [21] H. Long, M. Chen, and G. C. Schatz, "Cooperative DNA Melting in DNA Linked Gold Nanoparticle Aggregates," presented at Foundations of Nanoscience, Self-Assembled Architectures and Devices, Snowbird, UT, 2004.
- [22] F. Pierce, C. M. Sorensen, and A. Chakrabarti, "Aggregation-Fragmentation in a Model of DNA-Mediated Colloidal Assembly," *Langmuir*, vol. 21, pp. 8992-8999, 2005.
- [23] U. Christensen, N. Jacobsen, V. K. Rajwanshi, J. Wengel, and T. Koch, "Stopped-flow kinetics of locked nucleic acid (LNA)-oligonucleotide duplex formation: studies of LNA-DNA and DNA-DNA interactions," *Biochem J*, vol. 354, pp. 481-4, 2001.